RSC Advances

ROYAL SOCIETY OF CHEMISTRY

www.rsc.org/advances

Design and Synthesis of New Ruthenium Complex for Dye-Sensitized Solar Cells

M. G. Murali,[a] Xingzhu Wang,[b,c] Qing Wang,[b,c] Suresh Valiyaveettil,[a,b*]

[a] Department of Chemistry, National University of Singapore, 3 Science Drive 3, Singapore 117543

[b] NanoCore-NUSNNI, T-Lab Building, National University of Singapore, 5A Engineering Drive 1, Singapore 117411

[c] Department of Materials Science and Engineering, Faculty of Engineering, National University of Singapore, Singapore 117574

Abstract

A series of ruthenium complexes (MC1–MC3), incorporated with carbazole, fluorene and phenothiazine units with dipyrido[3,2-a:2',3'-c]phenazine is synthesized, characterized and their optical, electrochemical and photovoltaic properties are investigated. The observed differences in light-harvesting ability of the sensitizers are associated with the electron donor strength of the ancillary ligand used for preparing complexes. The dye-sensitized solar cell fabricated from complex MC–1 exhibited a power conversion efficiency of 6.18%. It is demonstrated that new molecular design and increase in molar absorption coefficient of the sensitizer improved the device performance.

Introduction

Dye-sensitized solar cells (DSSCs) have attracted considerable attention as a potential source of renewable energy owing to their low-cost of production and readily available components.[1,2] DSSCs were fabricated by adsorbing the dye molecules on a mesoporous oxide films such as TiO_2, ZnO or Nb_2O_5. The dye molecules acted as a sensitizer which broaden the light absorption window of the photoanode in the solar spectral region.[3–6] A few ruthenium complexes,[7–10] metal free organic dyes[11–15] and metalloporphyrins[12,16–18] have been developed and used as sensitizers in DSSCs. However, low power conversion efficiencies and shorter life time need to be improved for practical applications of DSSCs.[19]

Ruthenium complexes exhibit broad absorption and enhanced molar absorptivity with long-term stability.[20] One approach to improve the light-harvesting efficiency of the ruthenium complex is via extending the absorption range in the visible region via increasing the conjugation

length of the ligands used in metal complexes.[21,22] For example, replacing one of the 2,2'-bipyridyl-4,4'-dicarboxylic acid ligand (dcbpy) in the ruthenium compound of N719 and N3 with an extended π-conjugated ancillary ligand containing thiophene or alkoxy benzene derivatives, the absorption maximum was extended up to the longer wavelength region.[23,24] The compound dcbpy was used as a common anchoring group for metal complexes on TiO_2 substrate.[25]

In the present study, the area of coverage on the TiO_2 surface was extended by the design of linear dye molecules with metal coordinating sites which form complexes with ruthenium (Ru) metal ions. The 2,2'-bipyridine-4,4'-dicarboxylic acid is used as anchoring group for the metal complex. Such linear dye helps to cover a large area on the electrode, reduce aggregation, improve the stability, and enhance the efficiency of energy capture and transfer processes. The conceptual diagram is given in Figure 1.

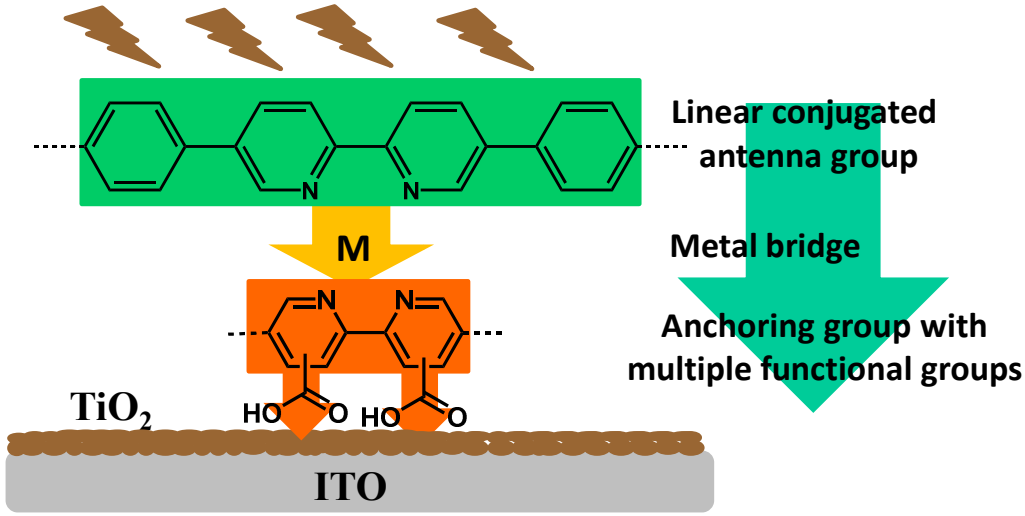

Figure 1 Conceptual diagram for the DSSC dyes designed and investigated in this study

Molecular structures of three new ruthenium complexes (MC1 – MC3) with linear light harvesting units such as carbazole, fluorene and phenothiazine attached to the dipyrido[3,2-a:2',3'-c]phenazine units are given in Figure 2. The optical, electrochemical properties, electron distribution of frontier orbital of the metal complexes and energy conversion performance of the synthesized ruthenium complex are investigated in detail.

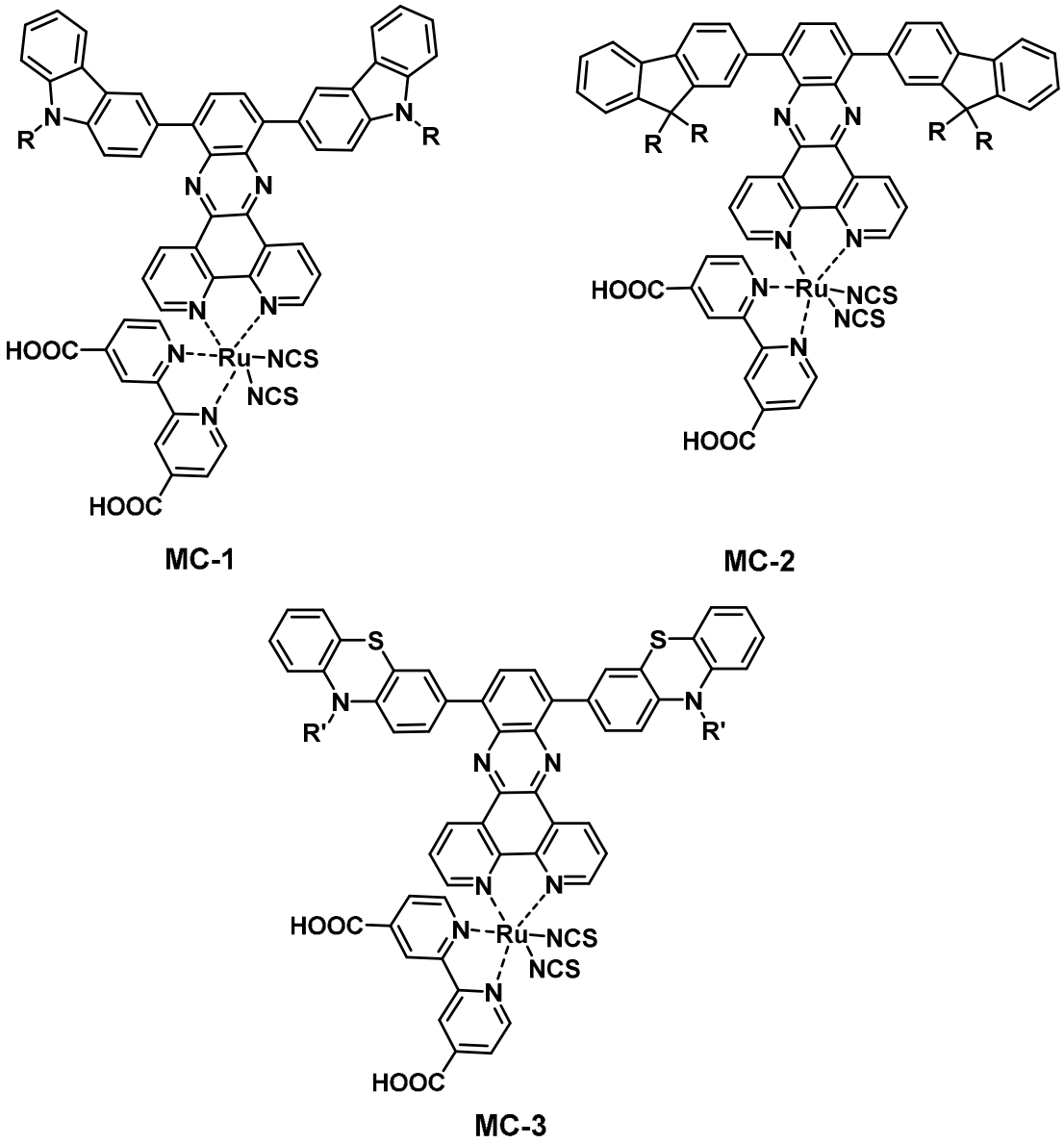

Figure 2 Target metal complexes (MC1 – MC3) synthesized and used for the DSSC studies.

Experimental section

Materials and instruments

The starting materials, 3-bromocarbazole, 2-bromofluorene, 3-bromo-10H-phenothiazine and 4,7-dibromobenzo[c]-1,2,5-thiadiazole were purchased from Sigma Aldrich and used as received. 3-Bromo-9-(2-ethylhexyl)-9H-carbazole (2A)[26], 9-(2-ethylhexyl)-3-(4,4,5,5-tetra methyl-1,3,2-dioxaborolane-2-yl)-9H-carbazole (3A)[26], 4,7-bis(9-(2-ethylhexyl)-9H-carbazol-3-yl)benzo[c][1,2,5]thiadiazole[27] and 1,10-phenanthroline-5,6-dione[28] were synthesized according to the reported procedure. All other chemicals and reagents were obtained from Sigma Aldrich

Ltd and used without further purification. Reactions were monitored by thin layer chromatography (TLC) using silica gel plates and products were purified on silica gel column using different solvents.

^{1}H and ^{13}C NMR spectra were recorded using a Bruker Avance AV300 (300/500/75 MHz) NMR spectrometer with TMS as internal reference. The following abbreviations were used to explain the signal multiplicities: s = singlet, d = doublet, t = triplet, m = multiplet, br = broad. ESI/EI/APCI mass spectrometry was used to confirm the mass of compound. UV-Vis absorption spectra were measured using a UV-1800 Shimadzu UV-VIS spectrophotometer with an optical filter that is calibrated at a bandwidth of 1 nm. Structural optimization and frontier orbital energy levels were calculated using density functional (DFT) model at B3LYP/6-31G(d) level. The LUMO and HOMO electron density plots were generated from the optimized structures using GaussView 5. Electrochemical studies of the metal complex were carried out using a CHI electrochemical analyzer. Cyclic voltammograms were recorded using a three-electrode cell system, with dye sensitized photoanode as working electrode, platinum wire as counter electrode and $Ag/AgNO_3$ as reference electrode (0.1M electrolyte solution with 0.01M AgNO3 in CAN). Photocurrent-voltage characteristics under AM 1.5G illumination at 95 mW cm^{-2} were carried out with a Keithley 2400 source meter and PVIV software package from Newport. Sunlight was obtained from a solar simulator (450 W, Newportclass A), and power was calibrated using a silicon reference cell. The photocurrent density – voltage traces of metal complex were measured under ambient conditions.[29] The active area of the cells was 0.119 cm^2 defined by a mask.

Preparation of TiO_2 electrode and DSSC device fabrication

Fluorine-doped indium tin oxide (FTO with a sheet resistivity of 8 – 10 Ω $square^{-1}$) coated glass plate was cleaned using 5% Decon 90 solution, deionized water and ethanol sequentially in an ultrasonic bath sequentially. On FTO plate, nanocrystalline TiO_2 (20 nm particle size) layers were deposited by successive screen printing using a TiO_2 paste (Dyesol, DSL 18-NR). A layer of larger TiO_2 particles (400 nm particle size, WER-O paste, Dyesol) was deposited on top of the transparent layer to increase light scattering on the TiO_2 layer. Thereafter, the electrode was gradually heated at 125 °C for 10 min, at 325 °C for 10 min, at 375 °C for 10 min, at 450 °C for 15 min and at 500 °C for 15 min. The electrodes were soaked in 40 mM solution of $TiCl_4$ in distilled water for 30 min at 75 ºC, washed with water and dried under ambient condition. The

prepared electrodes were immersed in a sensitizer (0.3 mmol) solution in DMF : t-BuOH mixture (3 : 1 v/v) for 24 h, followed by washing with DMF prior to cell assembly. A platinum thin film (thickness = 100 nm) deposited on a FTO coated glass plate was used as the counter electrode. The electrolyte composed of 0.5 M lithium iodide, 0.05 M iodine and 0.5 M 4-tert-butylpyridine in CH_3CN, was injected through a hole at the platinized FTO in a partial vacuum. Finally, the device was used for testing the performance of DSSCs.

Synthesis of ligands and the metal complex

Synthesis and characterization data of compounds, 2A – 2C, 3A – 3C and 4A – 4C are achieved using reported procedures and the details are summarized in the supplementary information. The synthetic route for compound 6A and target sensitizer, MC1 is given in Scheme 1. Similar synthetic schemes were used for MC2 and MC3 (see supporting information, Scheme 2 and Scheme 3).

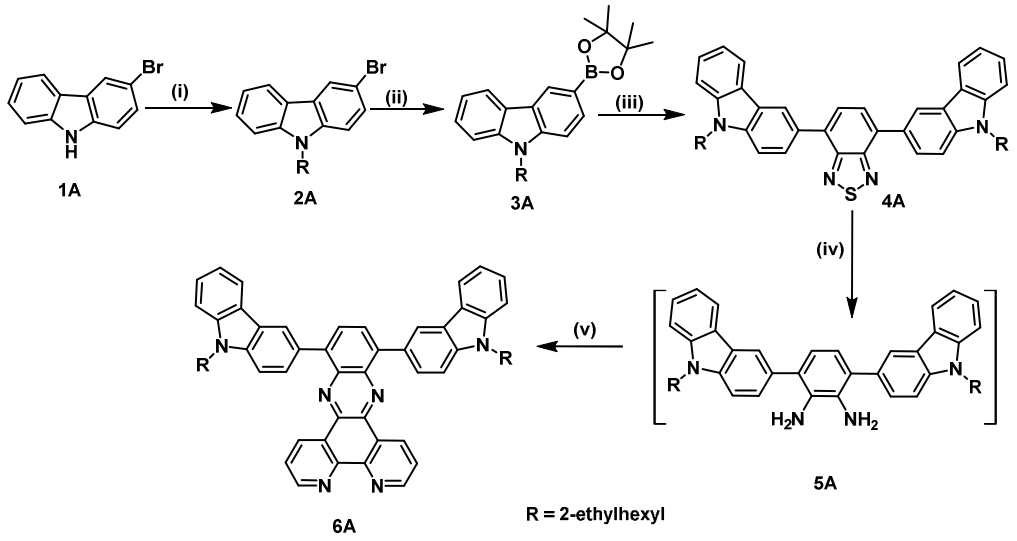

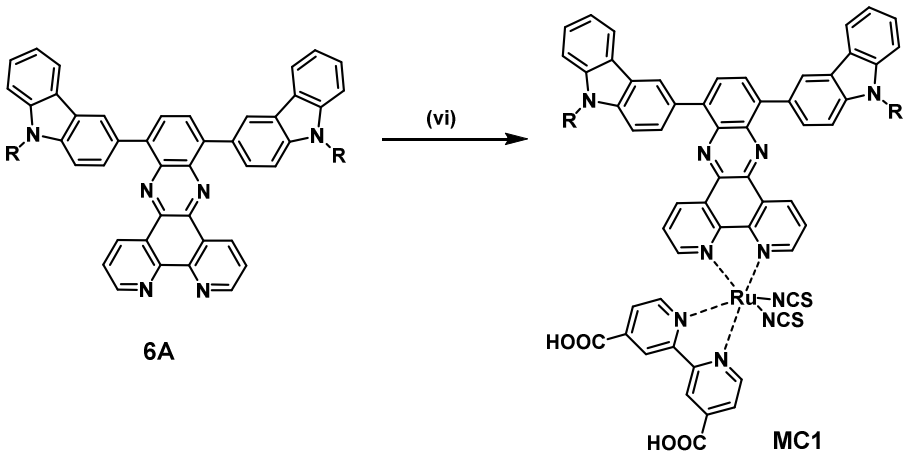

Scheme 1. Synthetic route for MC1; (I) KOH, RBr, DMF, room temperature, 12 h; (ii) Bis(pinacolato)diboron, CH_3COOK, $Pd(dppf)Cl_2.CH_2Cl_2$, 1,4-dioxane, 80 °C, 18 h, (iii) 4,7-dibromo-2,1,3-benzothiadiazole, K_2CO_3, $Pd(PPh_3)_4$, THF:H_2O, reflux, 24 h; (iv) Zn, acetic acid, 70 °C, 6 h; (v) 1,10-phenanthroline-5,6-dione, acetic acid, 70 °C, 12 h, (vi) Dichloro(p-cymene)ruthenium(II) dimer, 2,2'-bipyridine-4,4'-dicarboxylic acid, NH_4NCS, DMF, reflux.

Synthesis of Compound 6A

Compound 4A (0.28 g, 0.4 mmol) was dissolved in 10 ml of glacial acetic acid, followed by adding zinc dust (1.02 g, 16 mmol) in one portion, stirred at 70 °C for 6 h and filtered to remove the solid residue. The obtained crude compound, diamine 5A was treated with 1,10-phenanthroline-5,6-dione (85 mg, 0.4 mmol) and the resulting solution was stirred at 70 °C for 12 h. Reaction mixture was poured into ice water and extracted with chloroform (3 x 25 ml). The organic phase was washed with water several times, dried over anhydrous Na_2SO_4 and concentrated. The crude product was purified using silica gel column chromatography with dichloromethane: methanol (99:1) as eluent to obtain compound 6A as a red solid (0.2 g, yield 62 %). Similar procedure was followed for the synthesis of ligand 6B and 6C.

Compound 6A: ^{1}H NMR ($CDCl_3$, 300 MHz, δ ppm): 9.4 (d, 2H), 9.2 (d, 2H), 8.8 (d, 2H), 8.24 (s, 2H), 8.19 (d, 2H), 8.1 (d, 2H), 7.66 (d, 4H), 7.54 (d, 4H), 7.32 (d, 2H), 4.34 (d, 4H), 2.27–2.20 (m, 2H), 1.52–1.25 (m, 16H), 1.01 (t, 6H), 0.92 (t, 6H). ^{13}C NMR ($CDCl_3$, 75 MHz, δ ppm): 152.08, 148.36, 141.41, 140.71, 140.64, 139.66, 139.56, 133.80, 130.65, 129.08, 127.87, 125.77, 124.01, 123.35, 123.21, 122.85, 120.26, 119.13, 109.26, 108.44, 47.67, 39.59, 31.16, 28.93, 24.51, 23.19, 14.16, 11.02. HR-MS (APCI, *m*/*z*): calcd. for $C_{58}H_{57}N_6$ ([M+1]), 837.4639; found, 837.4646.

Compound 6B: ^{1}H NMR ($CDCl_3$, 300 MHz, δ ppm): 9.4 (d, 2H), 9.24 (d, 2H), 8.08 (d, 2H), 7.96 (d, 2H), 7.82 (d, 4H), 7.68 (d, 2H), 7.44 (d, 4H), 7.32 (d, 4H), 2.1 (t, 8H), 0.72 (br s, 4H), 0.9-0.86 (m, 32H), 0.59 (t, 12H), 0.46 (t, 12H). ^{13}C NMR ($CDCl_3$, 75 MHz, δ ppm): 152.44, 150.93, 148.25, 141.14, 140.01, 137.10, 134.27, 130.71, 128.20, 126.92, 126.62, 125.70, 124.45, 119.89, 119.16, 55.21, 44.81, 35.04, 34.08, 32.22, 31.42, 29.82, 28.46, 27.33, 22.85, 14.14, 14.07, 10.57. HR-MS (APCI, *m*/*z*): calcd. for $C_{76}H_{91}N_4$ ([M+1]), 1059.7238; found, 1059.7245 (error: -0.7 ppm).

Compound 6C: ^{1}H NMR ($CDCl_3$, 300 MHz, δ ppm): 9.09 (t, 5H), 7.85 (s, 2H), 7.64–7.59 (m, 8H), 7.0 (br, s, 7H), 3.98 (t, 4H), 1.96 (br, s, 4H), 1.41–1.25 (m, 12H), 0.95 (t, 6H). ^{13}C NMR ($CDCl_3$, 75 MHz, δ ppm): 151.60, 146.66, 139.37, 138.49, 133.71, 129.82, 127.23, 127.11,

124.16, 115.38, 114.48, 66.94, 60.24, 31.44, 29.55, 26.66, 22.53, 14.06, 13.92. HR-MS (APCI, *m*/*z*): calcd. for $C_{54}H_{49}N_6S_2$([M+1]), 845.3455; found, 845.3452.

Synthesis of target compound MC–1

Compound 6A (0.1 g, 0.11 mmol) and dichloro(p-cymene)ruthenium(II) dimer (36.5 mg, 0.055 mmol) were dissolved in 5 ml anhydrous DMF under inert atmosphere. The reaction mixture was heated at 80 °C for 4 h, followed by the addition of 2,2′-bipyridine-4,4′-dicarboxylic acid (26 mg, 0.11 mmol). Reaction mixture was heated at 150 °C for another 4 h under dark, excess NH_4NCS (91 mg, 1.2 mmol) was added, stirred for 5 h, poured into ice water and the black residue was filtered off. The excess NH_4NCS was removed by washing with water, followed by methanol. The crude product was further purified by repeated re-precipitation from chloroform: methanol (1:9) mixture to obtain the target compound MC–1 as a black powder (60 mg, yield 38 %). MC–2 and MC–3 were synthesized using similar procedures.

MC–1: ^{1}H NMR (DMF, 500 MHz, δ ppm): 9.88 (s, 1H), 9.58 (s, 1H), 9.31 (s, 1H), 9.1 (s, 1H), 8.77 (s, 1H), 8.48 (d, 1H), 8.29 (d, 2H), 8.12 (s, 2H), 7.87 (d, 2H), 7.81 (d, 2H), 7.73 (d, 4H), 7.65–7.6 (m, 4H), 7.53 (t, 4H), 7.26 (t, 2H), 4.55 (d, 4H), 1.99–1.93 (m, 2H), 1.44–1.4 (m, 16H), 0.9–0.82 (m, 12H). MS (ESI): (M_w=1298.5) found m/z = 1297.2 [M+]

MC–2: ^{1}H NMR (DMF, 500 MHz, δ ppm): 9.85 (s, 1H), 9.8 (d, 1H), 9.61 (d, 1H), 9.33 (s, 1H), 9.15 (s, 1H), 8.56 (d, 1H), 8.51 (d, 1H), 8.54–8.51 (m, 4H), 8.01 (d, 1H), 7.85–7.81 (m, 4H), 7.72 (d. 2H), 7.66 (d. 2H), 7.59 (s, 2H), 7.54 (t. 2H), 7.70–7.42 (m, 4H), 2.3–2.24 (m, 8H), 0.98–0.9 (m, 32H), 0.76 (br s, 4H), 0.68–0.64 (m, 12H), 0.61–0.56 (m, 12H). MS (ESI): (M_w=1521) found m/z = 1519.7

MC–3: ^{1}H NMR (DMF, 500 MHz□, δ□ppm): 9.79 (s, 1H), 9.5 (s, 1H), 9.17 (s, 1H), 9.07–8.97 (m, 4H), 8.37 (s, 1H), 8.10 (d, 2H), 7.79–7.71 (m, 4H), 7.44–7.36 (m, 4H), 7.28–7.24 (m, 4H), 7.19–7.09 (m. 6H), 4.04 (t, 4H), 1.86–1.80 (m, 4H), 1.26–1.16 (m, 12H), 0.82–0.74 (t, 6H). MS (ESI): (M_w=1306.5) found m/z = 1305.1 [M+].

Results and Discussion

Synthesis of target molecules

Three new precursor compounds, 6A – 6C, were synthesized using established procedures and used to prepare the target dye molecules, MC1 – MC3. In a typical procedure, N-alkylation of 3-bromocarbazole (1A) using KOH as a base in DMF solvent at room temperature to get 3-bromo-

9-(2-ethylhexyl)-9H-carbazole 2A. Subsequent Miyaura borylation reaction[26] of compound 2A (2B for MC–2 and 2C for MC–3) with bis(pinacolato)diborane was carried out using KOAc as a base and Pd(dppf)Cl_2.CH_2Cl_2 as a catalyst in 1,4-dioxane to obtain compound 3A in good yield. Compounds 4A was prepared via Suzuki Miyaura coupling reaction[27] of corresponding mono boronic acid pinacol ester compound 3A and 4,7-dibromobenzo[c]-1,2,5-thiadiazole. The compound 4A was reduced with zinc dust in glacial acetic acid to yield corresponding diamine, 5A. Since the diamine was unstable, it was used as such for the next step and treated with 1,10-phenanthroline-5,6-dione in glacial acetic acid at 70 ºC for 12 h to yield ligand 6A. Similarly, ligand 6B and 6C were prepared from appropriate starting materials. All intermediate compounds and ligands were purified using silica column chromatography. ^{1}H NMR and mass spectra of free ligands are presented in the supplementary data (Figure S1 and S2).

To prepare the target molecules, MC1 – MC3, dichloro(p-cymene)ruthenium(II) dimer and 2,2′-bipyridine-4,4′-dicarboxylic acid were treated with appropriate amounts of the ligands (6A – 6C) in anhydrous DMF under inert atmosphere (Scheme 1).[20,22] The crude complexes were further purified by successive re-precipitation using chloroform: methanol solvent mixture. The products were partially soluble in solvents such as chloroform, dichloromethane, THF, methanol, DMSO and completely soluble in DMF. The sensitizers (MC1 – MC3) were characterized using ^{1}H NMR and electrospray ionization (ESI) mass spectrometry.

Optical properties

The absorption and emission spectra of compounds 6A – 6C in DMF solution are given in Figure 3. The ligands exhibited two high energy absorption bands between 300 – 390 nm region (at 295 and 383 nm for 6A, 310 and 385 nm for 6B, 337 and ~382 for 6C) are assigned to the intra-ligand π–π* transitions of electron donor chromophores,[30] whereas, the absorption maxima observed at 472, 436 and 490 nm in the longer wavelength region, are assigned to n-π* absorption bands.[20,22] Further, n-π* absorption band of compound 6C is red shifted by 18 and 54 nm as compared to that of compound 6A and 6B, respectively. The observed red shift could be attributed to the stronger electron donating ability of phenothiazine unit in compound 6C.[31] Also, emission maxima were observed at 632, 565 and 614 nm, for 6A, 6B and 6C, respectively.

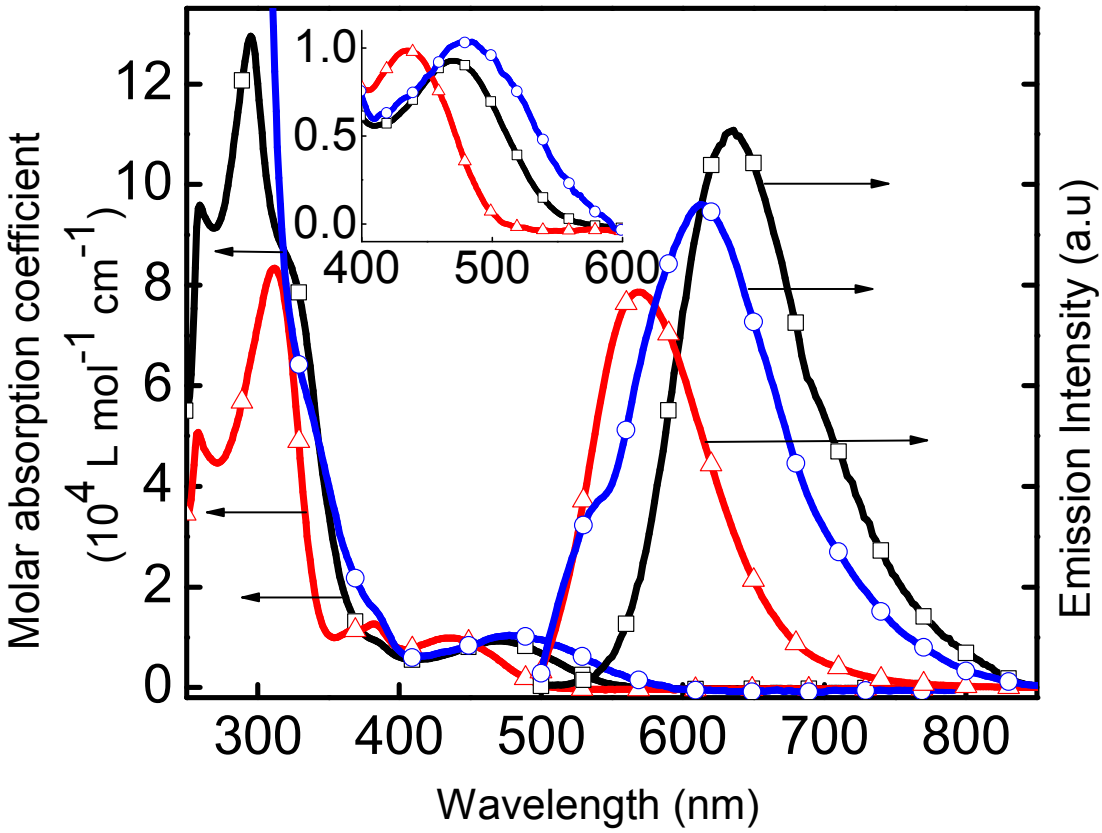

Figure 3 UV-Vis absorption (left) and emission (right) spectra of free ligands, 6A – 6C in DMF, (—□— 6A,—△— 6B, —○— 6C, inset: part of absorption spectra from 400 – 600 nm is enlarged for clarity).

The absorption and emission spectra of the complexes MC1 – MC3 in DMF solution are given in Figure 4, and summarized in Table 1. As shown in Figure 4, the sensitizers showed broader absorption maxima in the region of 300 to 400 nm owing to the intra-ligand π–π* transition.[20] Further, the absorption spectra of the compound 6A – 6C are dominated by metal to ligand charge transfer transition and the maxima are centered at 505, 471 and 513 nm for MC1 – MC3, respectively.[22] The lowest energy metal to ligand charge transfer transition band of MC–3 is red shifted about 8 and 42 nm as compared to that of MC–1 and MC–2, respectively. Here, the stronger electron donor unit phenothiazine in the ancillary ligand 6C of MC–3 lowers the metal to ligand charge transfer transition between metal center and the anchoring ligand. MLCT is the dominant factor for determining the efficiency of photosensitizer in DSSCs and increasing the

strength of the electron donor in the ancillary ligand of the metal complex, its MLCT transition will be driven to a lower energy and the dye will have a higher efficiency when used in DSSCs.[22] On the other hand, the molar absorption coefficient of the intra-ligand π–π* and MLCT band of MC–3 is lower than those of MC–1 and MC–2 (Table 1). These results indicate that enhancing the donor strength of the ancillary ligand does not increase the intensity of MLCT band, but shift to a lower energy region. This may lead to the decrease in device performance for MC–3. The emission maxima of target molecules were obtained by exciting at the respective low energy MLCT absorption bands, emission maxima appeared at 685, 600 and 560 nm, respectively, for MC1 – MC3.

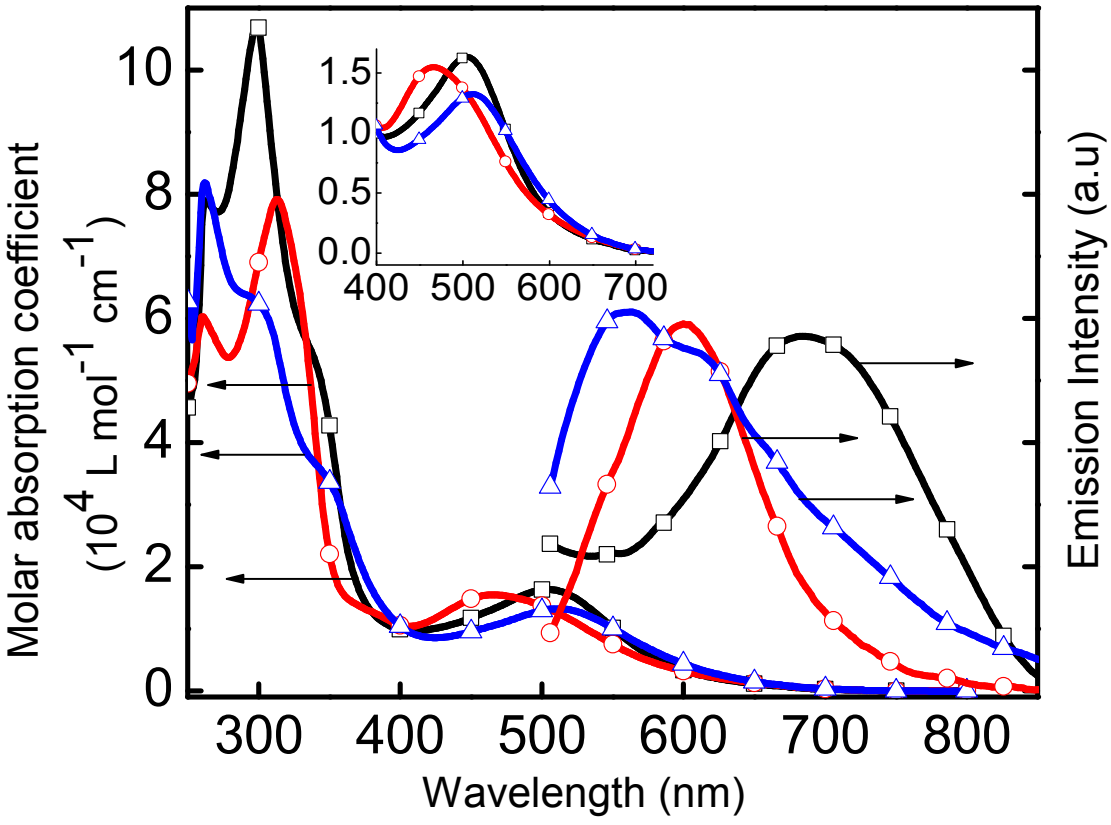

Figure 4 UV-Vis absorption (left) and emission spectra (right) of MC1–MC3 in DMF (—□— MC–1,—○— MC–2, —△— MC–3, inset: part of absorption spectra from 400 – 600 nm is enlarged for clarity).

The target molecular complexes MC1 – MC3 were adsorbed on a 2.5 μm transparent TiO_2 thin film which showed features similar to those of the corresponding absorption spectra in

solution state, but exhibited a blue-shift as a result of deprotonation of −COOH group on TiO_2 surface and presumably H-aggregate formation (Figure 5).[32]

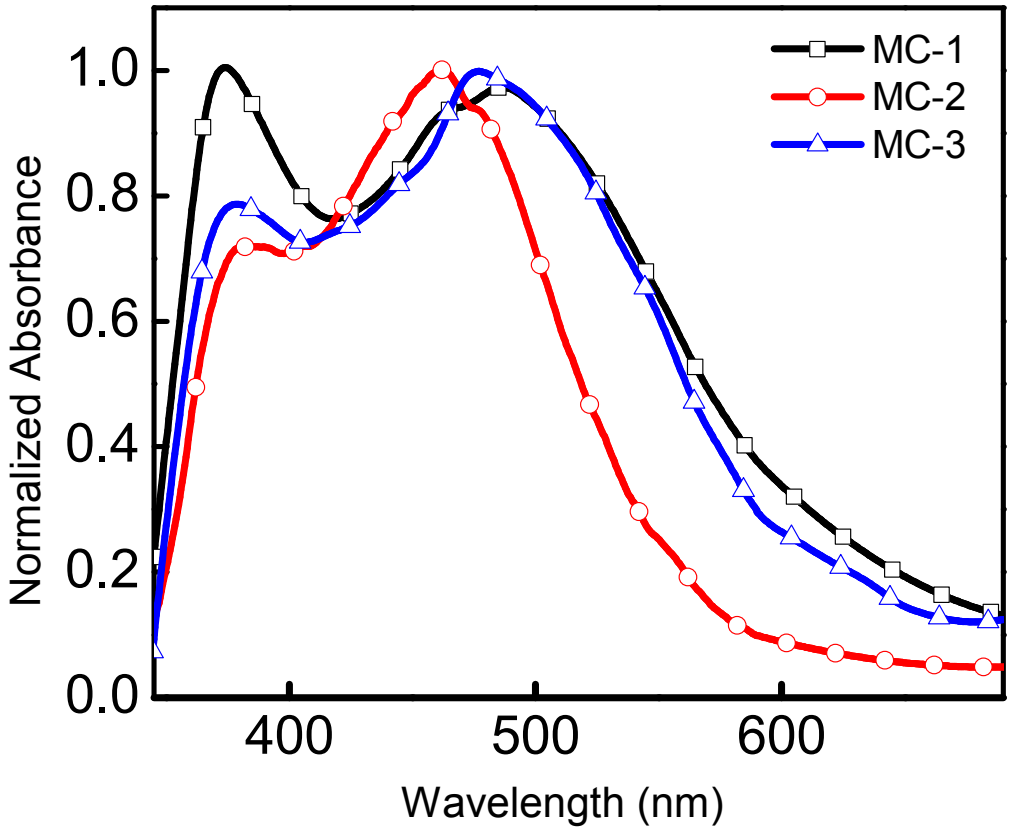

Figure 5 UV-Vis absorption spectra of MC1 – MC3 adsorbed on transparent mesoporous TiO_2 films

Electrochemical properties

To use dye molecule as a sensitizers in DSSCs, its band structure should match with the energy level of the semiconductor anode and the redox electrolyte or the hole conductor. That is to say, to minimize energetic losses during the electron-transfer reaction, the energy level of the excited state of dye should be matched with the TiO_2 conduction band. Also its redox potential should be sufficiently positive that it can be regenerated via electron donation from a redox electrolyte, such as I_3^-/I^-. Cyclic voltammograms (CV) of MC1 – MC3 were recorded on TiO_2 film with 0.1 M tetrabutylammonium hexafluorophosphate as the electrolyte at a scan rate of 100 mV s^{-1}. For calibration, the redox potential of ferrocene/ferrocenium (Fc/Fc+) was measured under the same condition and observed at 0.14 V *vs* $Ag/AgNO_3$ electrode. It was assumed that the redox potential of Fc/Fc+ has an absolute energy level of −4.80 eV in vacuum.[33,34] The HOMO and

LUMO energy levels of sensitizers were derived from oxidation/reduction potentials of the target molecules and summarized in Table 1.[35]

Two oxidative peaks are observed for the metal complex (Figure S4, supplementary data). The first oxidation peak is assigned to the oxidation of the metal center, and the second peak comes from the oxidation of free ligand.[36] The oxidation potential (E_{oxd}) of the metal center is estimated to be 0.57 and 0.68 V, respectively, for MC–1 and MC–2, whereas, the oxidation peak of metal centre observed for MC–3 at 0.45 V is cathodically shifted by 0.21 V indicating the electron-rich nature of the compound 6C. The second oxidation potential is situated at 0.81, 1.02 and 0.9 V, for MC–1, MC–2 and MC–3, respectively. It was observed that CV of the metal complexes is not electrochemically reversible. The reduction potentials (E_{red}) were determined by subtracting the optical energy band gap of the metal complex on TiO_2 film (E_g) from E_{oxd} and are found to be –1.3 V for MC–1, –1.18 V for MC–2 and –1.41 V for MC–3. The HOMO and LUMO energy levels are estimated to be –5.01 and –3.15 eV for MC–1, –5.1 and –3.24 eV for MC–2 and –4.92 and –3.06 eV for MC–3.

Table 1.Optical and electrochemical data of MC1–MC3

Sensitizer	**λ_{max}/nm (ε/L mol^{-1} cm^{-1})**	**λ_{emm}/nm**	***E*$_{oxd}$ of Ru $^{III/II}$ [V]**	**E_{oxd}^{on}(V)/ HOMO (eV)**	**E_{red}(V)/ LUMO (eV)**
MC–1	298 (107180 ± 80) 341 (52600 ± 60) 505 (16300 ± 30)	685	0.57	0.35/–5.01	–1.3/–3.15
MC–2	313 (78600 ± 70) 471 (15510 ± 50)	600	0.68	0.44/–5.1	–1.18/–3.24
MC–3	300 (61880 ± 90) 346 (34600 ± 60) 513 (12620 ± 45)	560	0.45	0.26/–4.92	–1.41/–3.06

E_{red} was calculated by the formula: $E_{red} = E_{oxd} - E_g$. The absorption onset of the each metal complex on TiO_2 film was used to calculate the energy gap (E_g). HOMO and LUMO energy levels were calculated using formula, HOMO [eV] = E_{oxd}^{on}–$E_{Fc/Fc+}$ + 4.8; LUMO [eV] = HOMO – E_g. E_{oxd}^{on} is the onset oxidation potential. i.e potential at which oxidation of the metal complex starts, whereas E_{oxd} is the oxidation potential at specific voltage.

Energy level diagrams of MC1 – MC3, TiO_2 and I_3^-/I^- electrolyte are illustrated in Figure 6. The position of the HOMO level of the metal complex is sufficiently below the energy level of iodide/triiodide couple redox mediator (–4.8 eV) allowing dye regeneration. Nevertheless, the position of the LUMO level is closer to the TiO_2 conduction band (–4.0 eV) to facilitate efficient electron transfer from the excited dye to TiO_2.[20]

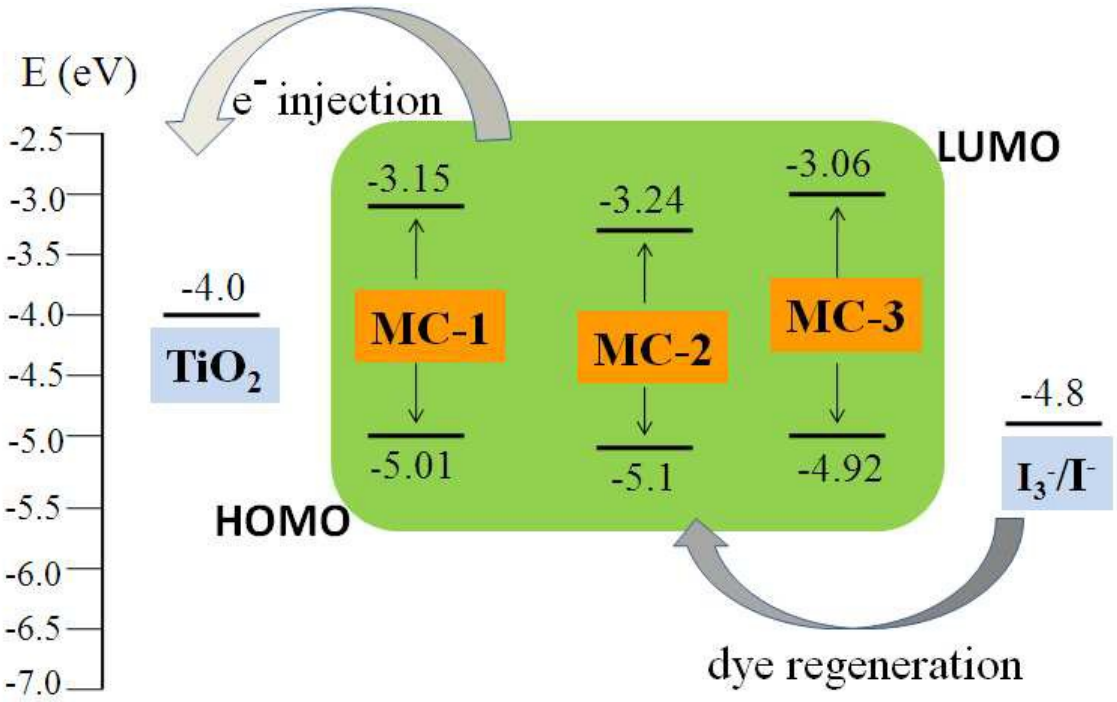

Figure 6 Energy level diagrams of MC1 – MC3, TiO_2 and I_3^-/I^-

Density functional theory calculations

In order to get insight into the geometrical configuration and electron distribution of the frontier orbitals of the sensitizer, density functional theory (DFT) calculations were carried out using a B3LYP/6-31G level program.[37] The optimized ground state molecular structure and orbital profiles for the HOMO and LUMO of the target complex MC–1 are presented in Figure 7. It is observed that the HOMO of the target dyes is distributed on the ruthenium metal and the NCS ligands. Within the NCS ligands, the amplitude is primarily located on the sulfur atom. The LUMO and HOMO–1 of MC–1 are localized homogeneously on the dcbpy ligands, facilitating electron injection from the excited Ru metal complex to the TiO_2. Molecular orbital profile of all metal complexes is similar in structure and distribution (Figure 7 and Supporting Information,

Figure S5 for MC–2 and MC–3). The charge transfer between the metal and ligands is not expected to contribute to the conversion efficiency of the DSCs.[22] It is observed that LUMO+1of MC–1 and LUMO of MC–2 and MC–3 are localized more on their ligand part. This leads to decrease in the strength of the MLCT transition between the metal and the dcbpy ligand, which is further supported by the absorption studies of the sensitizer, where decrease in intensity of MLCT band of metal complexes was observed.

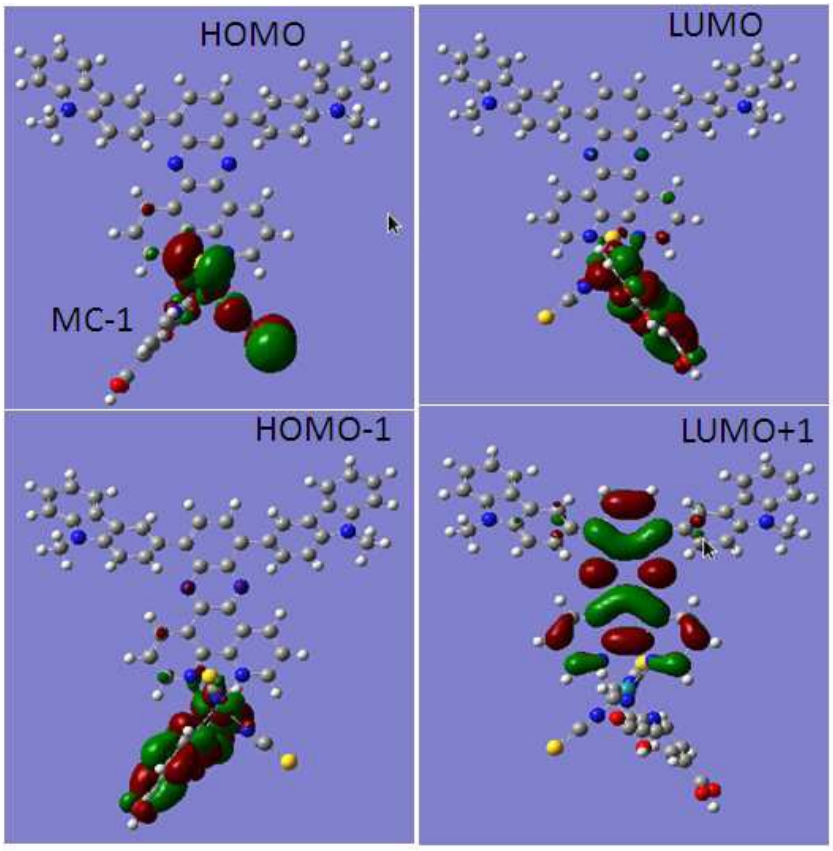

Figure 7 Graphical representation of the frontier orbitals of MC–1calculated at the B3LYP/6-31G (d,p) level of theory. Atoms in red, yellow, brown, blue, and gray correspond to oxygen, sulfur, carbon, nitrogen, and ruthenium, respectively.

Solar cell performance

The photocurrent density–voltage traces of MC1 – MC3 incorporated solar cells are shown in Figure 8 and the detailed device data are summarized in Table 2. The sensitized solar cell of MC–1 exhibit a short–circuit photocurrent density (J_{sc}) of 11.49 mA cm^{-2}, an open–circuit potential (V_{oc}) of 0.71 V and a fill factor (*FF*) of 0.75, corresponding to an overall conversion efficiency (η) of 6.18 % under AM 1.5 sunlight illumination. The power conversion efficiency of

MC–2 and MC–3 based solar cell is 3.57 and 1.62 %, respectively. The MC–2 based solar cell showed low device performance as compared to that of MC–1 and this could be attributed to its weak light harvesting ability in the longer wavelength region (Figure 4). A decrease in photocurrent density was observed for MC–2 (7.27 mA cm^{-2}) than that of MC–1. On the other hand, MC–3 based device showed a low device performance, though its MLCT band is at lower energy region than those of other two metal complexes. The obtained results agree with the fact that the molar absorption coefficient of MLCT band in MC–3 is lower than those of MC–1 and MC–2 (Table 1). The open–circuit voltage value of MC–1 and MC–2 based device is almost similar, but the value for MC–3 is lower than those of the other two complexes. This could be contributed to poor device performance for MC–3 based DSSC devices. It is known that the open–circuit voltage of the device depends on the Fermi level energy of TiO_2. Higher the proton concentration on the surface, the lower the Fermi level energy of the TiO_2 nanocrystallite.[22,38] The low efficiency for MC–3 is mainly attributed to the lower J_{sc} value and molar absorption coefficient.

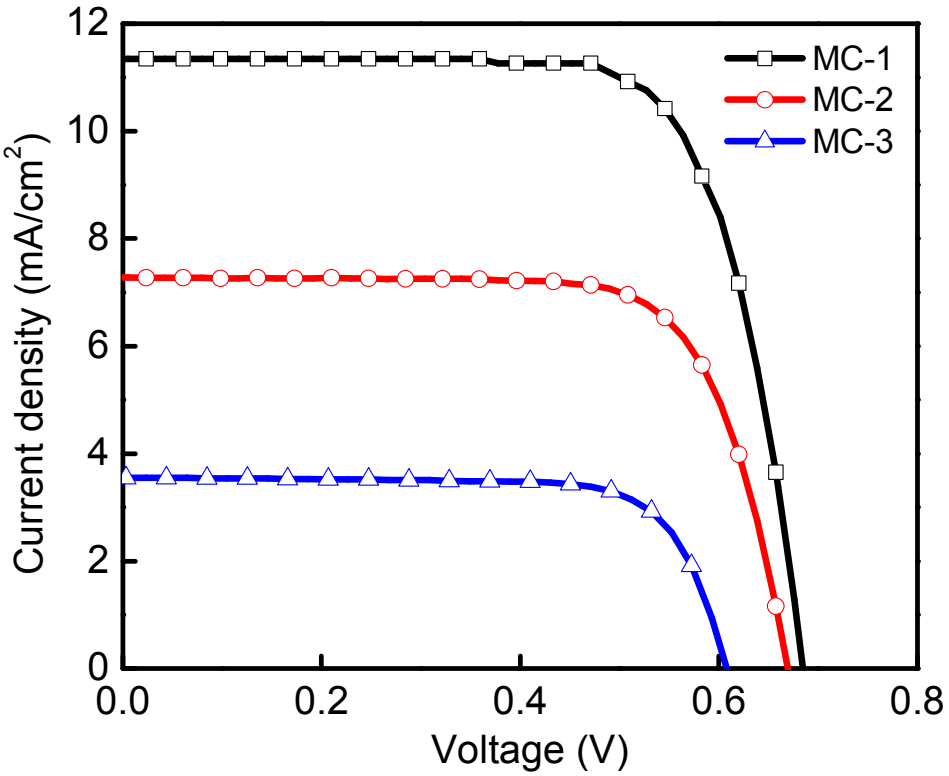

Figure 8 Current density–voltage characteristics of photovoltaic devices with MC1 – MC3 as sensitizer under AM 1.5 simulated sunlight (95 mW cm^{-2}) illumination. (Cell active area: 0.119 cm^2)

Table 2. Photocurrent density (J_{sc}), open–circuit potential (V_{oc}), fill factor (FF) and power conversion efficiency (η) of MC1–MC3 sensitized devices

Sensitizer	J_{sc} [mA/cm^2]	V_{oc} [V]	FF	η (%)
MC–1	11.49	0.71	0.75	6.18
MC–2	7.27	0.66	0.73	3.57
MC–3	3.55	0.60	0.75	1.62

Conclusions

In conclusion, a new series of ruthenium complexes, MC1–MC3 incorporating carbazole, fluorene and phenothiazine units attached to dipyrido[3,2-a:2',3'-c]phenazine were synthesized, characterized and employed as sensitizers in DSSCs. Increasing the electron donor strength of the ancillary ligand improved the overall spectral response of the sensitizer in the longer wavelength region. The device based on MC–1 sensitizer showed a short–circuit photocurrent density (J_{sc}) of 11.49 mA cm^{-2}, an open–circuit voltage (V_{oc}) of 0.71 V, and a fill factor (FF) of 0.75, corresponding to an overall conversion efficiency (η) of 6.18 %. Such metal complexes are useful towards understanding the mechanism of DSSCs and enhance the performance of such devices in the future.

Acknowledgements

The authors wish to thank the Ministry of Education for funding support (R-143-000-570-112) and department of chemistry at the National University of Singapore for technical support.

References:

1 B. O'Regan and M. Gratzel, *Nature*, 1991, **353**, 737–740.
2 M. Gratzel, *Nature*, 2001, **414**, 338–344.
3 T. Yoshida, K. Terada, D. Schlettwein, T. Oekermann, T. Sugiura and H. Minoura, *Adv. Mater.*, 2000, **12**, 1214–1217.
4 T. Yoshida and H. Minoura, *Adv. Mater.*, 2000, **12**, 1219–1222.
5 S.-D. Burnside, V. Shklover, C. Barbé, P. Comte, F.Arendse, K. Brooks and M. Grätzel, *Chem. Mater.*, 1998, **10**, 2419–2425.
6 V. C. Anitha, A. N. Banerjee, S. W. Joo and B. K. Min, *J. Ind. Eng. Chem.*, 2015, **29**, 227-237.
7 M. K. Nazeeruddin, F. De Angelis, S. Fantacci, A. Selloni, G. Viscardi, P. Liska, S. Ito, B. Takeru and M. Grätzel, *J. Am. Chem. Soc.*, 2005, **127**, 16835–16847.
8 Y. Cao, Y. Bai, Q. Yu, Y. Cheng, S. Liu, D. Shi, F. Gao and P. Wang, *J. Phys. Chem. C*, 2009, **113**, 6290–6297.

9 K. Hara, K. Sayama, Y. Ohga, A. Shinpo, S. Suga and H. Arakawa, *Chem Commun*, 2001, 569–570.

10 P.-Y. Su, J.-M. Liu, X.-L. Lin, Y.-F. Chen, Y.- Shen, L.-M. Xiao, D.-B. Kuang and C. Y. Su, *Inorg. Chem. Front.*, 2015, **2**, 1040–1044.

11 S. Kim, J.-K. Lee, S.-O. Kang, J. Ko, J.-H. Yum, S. Fantacci, F. De Angelis, D. Di Censo, Md. K. Nazeeruddin and M. Grätzel, *J. Am. Chem. Soc.*, 2006, **128**, 16701–16707.

12 S. Mathew, A. Yella, P. Gao, R. Humphry-Baker, B. F. Curchod, N. Ashari-Astani, I. Tavernelli, U. Rothlisberger, M. K. Nazeeruddin and M. Grätzel, *Nat Chem*, 2014, **6**, 242–247.

13 L.-P. Zhang, K.-J. Jiang, G. Li, Q.-Q. Zhang and L.-M. Yang, *J Mater Chem A*, 2014, **2**, 14852–14857.

14 N. Manfredi, B. Cecconi and A. Abbotto, *Eur. J. Org. Chem.*, 2014, **2014**, 7069–7086.

15 Y. J. Chang, P.-T. Chou, Y.-Z. Lin, M. Watanabe, C.-J. Yang, T.-M. Chin and T. J. Chow, *J. Mater. Chem.*, 2012, **22**, 21704–21712.

16 A. Yella, H.-W. Lee, H. N. Tsao, C. Yi, A. K. Chandiran, M. K. Nazeeruddin, E. W.-G. Diau, C.-Y. Yeh, S. M. Zakeeruddin and M. Grätzel, *Science*, 2011, **334**, 629–634.

17 T. Bessho, S. M. Zakeeruddin, C.-Y. Yeh, E. W.-G. Diau and M. Grätzel, *Angew. Chem. Int. Ed.*, 2010, **49**, 6646–6649.

18 K. Ladomenou, T. N. Kitsopoulos, G. D. Sharma and A. G. Coutsolelos, *RSC Adv.*, 2014, **4**, 21379–21404.

19 U. Bach, D. Lupo, P. Comte, J. E. Moser, F. Weissortel, J. Salbeck, H. Spreitzer and M. Gratzel, *Nature*, 1998, **395**, 583–585.

20 A. Mishra, N. Pootrakulchote, M. K. R. Fischer, C. Klein, M. K. Nazeeruddin, S. M. Zakeeruddin, P. Bauerle and M. Gratzel, *Chem Commun*, 2009, 7146–7148.

21 C. Klein, Md. K. Nazeeruddin, P. Liska, Davide Di Censo, N. Hirata, E. Palomares, J. R. Durrant and M. Grätzel, *Inorg. Chem.*, 2005, **44**, 178–180.

22 C.-Y. Chen, H.-C. Lu, C.-G. Wu, J.-G. Chen and K.-C. Ho, *Adv. Funct. Mater.*, 2007, **17**, 29–36.

23 C.-Y. Chen, S.-J. Wu, C.-G. Wu, J.-G. Chen and K.-C. Ho, *Angew. Chem. Int. Ed.*, 2006, **45**, 5822–5825.

24 F. Gao, Y. Wang, J. Zhang, D. Shi, M. Wang, R. Humphry-Baker, P. Wang, S. M. Zakeeruddin and M. Gratzel, *Chem Commun*, 2008, 2635–2637.

25 M. Yanagida, L. P. Singh, K. Sayama, K. Hara, R. Katoh, A. Islam, H. Sugihara, H. Arakawa, M. K. Nazeeruddin and M. Gratzel, *J Chem Soc Dalton Trans*, 2000, 2817–2822.

26 B. Liang, S. Hu, Y. Liu, Z. Fan, X. Wang, W. Zhu, H. Wu and Y. Cao, *Dyes and Pigments*, 2013, **99**, 41–51.

27 X. Bi, W. Zuo, Y. Liu, Z. Zhang, C. Zeng, S. Xu and S. Cao, *Mater. Res. Bull.*, 2015, **70**, 865–875.

28 H. Shahroosvand, P. Abbasi, E. Mohajerani and M. Janghouri, *Dalton Trans*, 2014, **43**, 9202–9215.

29. B. Yang, O. Dyck, J. Poplawsky, J. Keum, A. Puretzky, S. Das, I. Ivanov, C. Rouleau, G. Duscher, D. Geohegan and K. Xiao, *J. Am. Chem. Soc.*, 2015, **137**, 9210–9213.

30 J. Geng, Y. Dai, X.-X. Wang, M.-Y. Hu, T. Tao and W. Huang, *Tetrahedron*, 2015, **71**, 654–662.

31 X. Ma, E. A. Azeem, X. Liu, Y. Cheng and C. Zhu, *J Mater Chem C*, 2014, **2**, 1076–1084.

32 Q. Qi, X. Wang, L. Fan, B. Zheng, W. Zeng, J. Luo, K.-W. Huang, Q. Wang and J. Wu, *Org. Lett.*, 2015, **17**, 724–727.
33 J. Pommerehne, H. Vestweber, W. Guss, R. F. Mahrt, H. Bässler, M. Porsch and J. Daub, *Adv. Mater.*, 1995, **7**, 551–554.
34 V. Gaidelis, E. Kamarauskas, T. Malinauskas, V. Getautis, R. Send, H. Wonneberger and I. Bruder, *RSC Adv.*, 2015, **5**, 82859–82864.
35 D. M. de Leeuw, M. M. J. Simenon, A. R. Brown and R. E. F. Einerhand, *Synth. Met.*, 1997, **87**, 53–59.
36 S.-Q. Fan, C. Kim, B. Fang, K.-X. Liao, G.-J. Yang, C.-J. Li, J.-J. Kim and J. Ko, *J. Phys. Chem. C*, 2011, **115**, 7747–7754.
37 C. Daul, E. J. Baerends and P. Vernooijs, *Inorg. Chem.*, 1994, **33**, 3538–3543.
38 J. Bisquert, D. Cahen , G. Hodes, S. Rühle and A. Zaban, *J. Phys. Chem. B*, 2004, **108**, 8106–8118.

Design and Synthesis of New Ruthenium Complex for Dye-Sensitized Solar Cells

M. G. Murali,[a] Xingzhu Wang,[b,c] Qing Wang,[b,c] Suresh Valiyaveettil,[a,b*]

Graphical Abstract